Optimization of Spatial Windshield Wiper Linkages by Using the Differential Evolution Method

Tsai-Jung Chen * and Tien-Shun Chung

Posted Date: 24 July 2024

doi: 10.20944/preprints202407.1845.v1

Keywords: Intelligent optimization algorithms; RSSR mechanics; Differential evolution algorithm

Article

Optimization of Spatial Windshield Wiper Linkages by Using the Differential Evolution Method

Tsai-Jung Chen [1]* and Tien-Shun Chung [2]

[1] Department of Mechanical Engineering, National Pingtung University of Science and Technology, Pingtung 912, Taiwan;
[2] Department of Vehicle Engineering, National Pingtung University of Science and Technology, Pingtung 912, Taiwan; benson89526 @gmail.com
* Correspondence: turtlechen29@mail.npust.edu.tw;

Abstract: This study developed a three-dimensional kinematic and dynamic model of a center-driven linkage system (CDLS). Force analysis was conducted to determine the required driving torque to ensure that the input link of the CDLS rotates at a constant speed with a certain angular velocity, even in the presence of frictional resistance torque. The primary objective was to optimize the maximum angular acceleration of the output links to reduce wiper noise. This optimization can enhance the stability of the linkage system while maintaining its operational functionality. In the adopted methodology, the frames of the fixed links are assumed to remain unchanged, and the input link is considered to operate at a constant angular speed and have a constant length. To meet standard vehicle windshield wiper requirements, 10 constraints were imposed on the optimization problem, which was solved using the differential evolution method. The lengths of both output links were reduced by over 10% after optimization.

Keywords: intelligent optimization algorithms; RSSR mechanics; differential evolution algorithm

1. Introduction

Spatial four-bar linkages are employed to achieve mechanical input–output relationships between spatially oriented axes of movement. A revolute–spherical–spherical–revolute (RSSR) spatial four-bar mechanism features two revolute joints of arbitrary orientation that are attached to a fixed link and two spherical joints that connect cranks to a coupler link. The analysis and development of these linkages are interesting and challenging problems. Numerous researchers have made significant contributions to the study of rigid-link RSSR mechanisms [1–12]. A center-driven linkage system (CDLS) comprises two RSSR linkage systems driven by a single central input link. In the present study, we developed a three-dimensional kinematic and dynamic model of a CDLS for windshield wipers. Chen et al. [13,14] proposed that appropriately reducing the magnitude of a wiper's acceleration (or deceleration) helps decrease vibrations, which can reduce unpleasant rubber wiper noises on vehicle windshields. We adopted the objective function and constraints presented in their study to optimize the link lengths in a wiper linkage system by employing a differential evolution (DE) search method.

DE was introduced by Storn and Price in 1995 [15–17] and rapidly gained widespread adoption because of its simplicity and experimental efficiency. Numerous variants of DE have been developed to enhance its optimization capabilities, including DE with trigonometric mutation [18], opposition-based learning (OBL) DE [19–21], DEGL (DE with global and local neighborhoods) incorporating neighborhood-based mutation [22], and self-adaptive DE [23–25]. These innovations have considerably bolstered DE's robustness and adaptability, making it a versatile tool for diverse optimization problems. The equilibrium optimizer, introduced by Faramarzi et al. [26], is inspired by the principles of dynamic and equilibrium states in physics. This algorithm has been demonstrated to outperform DE and other optimization techniques because it effectively balances the exploration and exploitation phases. In addition, Mallipeddi et al. [27] investigated various mutation strategies and parameter settings within DE and substantially improved its robustness and adaptability across various optimization scenarios. Wang et al. [28] conducted a scalability analysis of DE enhanced with generalized OBL and achieved significant performance gains for large-scale optimization tasks.

 doi:10.20944/preprints202407.1845.v1

Similarly, Choi et al. [29] introduced a stochastic variant of OBL for DE, which substantially enhanced the convergence speed and solution quality for numerical optimization problems.

Wang et al. integrated the gray wolf optimizer with DE to improve feature selection and demonstrated that their method was more effective than conventional DE and other methods were. Heidari et al. [30] explored integrating the Harris Hawks Optimization algorithm with DE and highlighted the superior efficiency of this integrated method for solving intricate engineering optimization challenges.

Collectively, the aforementioned studies underscore the versatility and effectiveness of DE for solving sophisticated optimization challenges in various domains. Ongoing enhancements to DE and the introduction of novel DE variants ensure the enduring relevance and applicability of DE in solving increasingly complex optimization problems. The objective function for optimization in this study is defined as follows:

$$\mathrm{f}(r_3, r_4, r_5, r_6) = \max_{0 \le \theta_2 \le 2\pi} |\alpha_4(r_2, r_3, r_4, \theta_2)| + \max_{0 \le \theta_2 \le 2\pi} |\alpha_6(r_2, r_5, r_6, \theta_2)| \quad (1)$$

where $\boldsymbol{\alpha_4}$ and $\boldsymbol{\alpha_6}$ represent the angular accelerations of the output links on the driver and passenger sides of the CDLS, respectively.

This optimization problem is subject to 10 constraints derived from typical requirements for vehicle windshield wipers. The aforementioned objective function is a function of the parameters of the connecting and output links on the driver and passenger sides of the CDLS. Additional details on this objective function are provided in Section 2. The input link of the CDLS is assumed to rotate at a constant speed with an angular velocity of 1 rad/s. Our optimization calculations for this linkage system indicate that the maximum angular acceleration of the output link on the driver side of the CDLS can be reduced by 13.64%. Additionally, the calculations show that the maximum angular acceleration of the output link on the passenger side can be reduced by 14.38%. In addition, we developed a dynamic model of the CDLS. Through force analysis, we determined the required motor torque to ensure that the input link of the CDLS rotates at a constant speed with a given angular velocity, even in the presence of frictional resistance torque.

2. Materials and Methods

A flowchart of our method is shown in Figure 1. This section discusses a kinematic model of the CDLS. Mathematical formulas based on this model were established for the angles, angular velocities, angular accelerations, and transmission angles of various parts of the CDLS. Numerical simulations of CDLS motion were then performed in MATLAB by using these mathematical formulas.

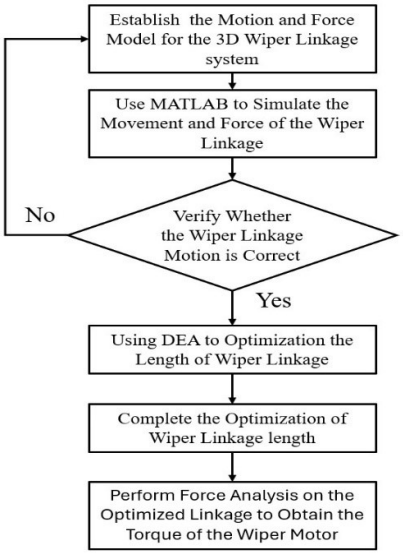

Figure 1. Flowchart of our research method.

 doi:10.20944/preprints202407.1845.v1

Mathematical formulas for $\alpha_4$and for α_6 are provided in Section 2.1. Section 2.2 presents the mathematical formulas for the magnitudes of the joint forces acting on each link and the driving torque of the motor. Finally, Section 2.3 describes the use of DE to minimize the objective function of the present study under the 10 considered constraints. Finally, this section discusses a dynamic model of the CDLS. This model and Euler's laws of motion can be used to determine the magnitudes of the joint forces acting on each link and the driving torque of the motor. The torque exerted by an external load on the output links is considered in the analysis to ensure that the crank rotates at a constant speed.

2.1. Wiper Linkage Motion Model

Figure 2 displays the structure of a CDLS. The vectors of the crankshaft's axis are not mutually parallel with the vectors of the output links of the wipers on both sides; therefore, the linkages cannot be simplified into a planar model. To precisely optimize the rod lengths and meet the requirements of practical applications, we established a simplified three-dimensional kinematic model of a CDLS (Figure 4). For this model, three Cartesian coordinate systems were established: XYZ , $X_1Y_1Z_1$, and $X_2Y_2Z_2$. Point A is the origin of coordinate system XYZ, and the motor shaft vector is aligned along the Z-axis. Link AB rotates in the XY plane around the Z-axis. Point D is the origin of coordinate system $X_1Y_1Z_1$, and Link CD rotates about the Z_1-axis within the X_1Y_1plane. Finally, point E is the origin of coordinate system $X_2Y_2Z_2$, and Link EF rotates about the Z_2-axis within the X_2Y_2 plane.

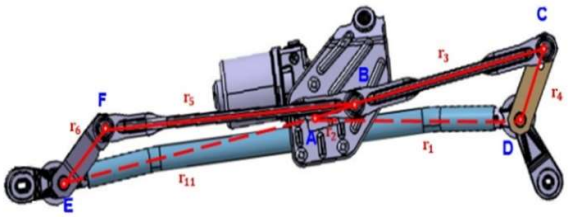

Figure 2. Structure of a CDLS.

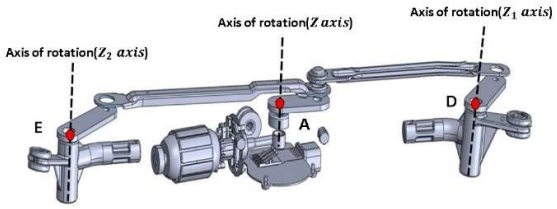

Figure 3. Rotating shafts, coordinate origins, and axes of rotation.

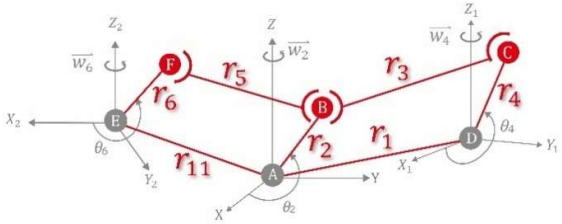

Figure 4. Simplified three-dimensional kinematic model of a CDLS.

The link components of the CDLS were measured in millimeters, and angles were measured in radians .

The linkage system, which includes Links AB, BC, CD, and AD, drives the wiper on the driver side of the CDLS. Link AD is fixed, and Link AB, commonly referred to as the crankshaft, is the input link that receives power to drive Links BC and CD. Link BC is a connecting link, and Link CD is the output link on the driver side of the CDLS. Link AB is the shortest link and can rotate 360°. The

 doi:10.20944/preprints202407.1845.v1

lengths of these four driver-side links must satisfy Grashof's law [14]. ABCD is a spatial four-bar linkage mechanism; points A, B, C, and D have a rotational joint R, spherical joint S, spherical joint S, and rotational joint R, respectively. This mechanism is commonly known as an RSSR mechanism. The angle μ_4 between Links BC and CD is commonly referred to as the transmission angle on the driver side of the CDLS [31], and μ_4 varies as the input link (Link AB) rotates. The mechanism achieves optimal efficiency (maximized effective torque) when the transmission angle is π/2 radians. Typically, the transmission angle must be able to vary from 40° to 140° [31].

The linkage responsible for driving the wiper on the passenger side of the CDLS comprises Links AB, BF, AE, and EF. Link AE is a fixed link, and Link AB is the input link (crankshaft) that powers Links BF and EF. Link BF and Link EF are the connecting and output links, respectively, on the passenger side of the CDLS, and the angle μ_6 between Links BF and FE is the transmission angle on the passenger side of the CDLS. For the driver side, the efficiency is optimized when the transmission angle is π/2 radians.

The lengths of Links AB, BC, CD, and AD are denoted as r_2, r_3, r_4 and r_1, respectively. In addition, the angles between Link AB and the *X*-axis, Link DC and the X_1-axis, and Link EF and the X_2-axis are denoted as θ_2, θ_4, and θ_6, respectively (refer to Figure 4). Similarly, the lengths of Links BF, FE, and AE are denoted as r_5 , r_6 , and r_{11} respectively. The lengths of Links AB, BC, CD, and AD (passenger-side links) must also satisfy Grashof's law. ABFE is also a spatial four- bar linkage mechanism with a rotational joint R, spherical joint S, spherical joint S, and rotational joint R at points A, B, F, and E, respectively (Figure 4).

The following paragraphs discuss the mathematical formulas for the established model.

2.1.1. Matrices for Three-Dimensional Rotations

The y_i-axis is defined as running horizontally left and right on the paper, and the z_i-axis is defined as running vertically up and down on the paper. The diagonal line represents the x_i-axis, which is perpendicular to the other two axes; its positive direction is out of the paper, and its negative direction is into the paper. The positive axes of the standard $x_iy_iz_i$ coordinate frame point in the out, right, and up directions (Figure 5). The standard definitions of the rotations about the three principle axes are first explained. Consider two right-handed rectangular coordinate systems with a common origin, as depicted in Figure 5. The coordinate system $x_jy_jz_j$ can be obtained from the coordinate system $x_iy_iz_i$ by performing a counterclockwise rotation about the z_i-axis by an angle θ. The sign of θ follows the right-hand rule: When the thumb points in the positive direction of the z_i-axis, a counterclockwise rotation from the x_i-axis to the x_j-axis indicates a positive θ value, whereas a clockwise rotation indicates a negative θ value. The coordinate transfer matrix is expressed as follows:

$$\left[C_{ij}{}^{(\theta)}\right] = \begin{bmatrix} cos(\theta) & sin(\theta) & 0 \\ -sin(\theta) & cos(\theta) & 0 \\ 0 & 0 & 1 \end{bmatrix}$$

where (θ) in the upper right corner of the square matrix indicates that the coordinate system $x_jy_jz_j$ is obtained by rotating the coordinate system $x_iy_iz_i$ about the z_i-axis by the angle θ. Two vectors in the $O_{x_iy_iz_i}$ and the $O_{x_jy_jz_j}$ systems, namely (x, y, z) and (x', y', z'), respectively, have the following relationship:

$$\begin{bmatrix} x' \\ y' \\ z' \end{bmatrix} = \left[C_{ij}{}^{(\theta)}\right] \begin{bmatrix} x \\ y \\ z \end{bmatrix}$$

As shown in Figure 6, the coordinate system $x_jy_jz_j$ can be obtained from the coordinate system $x_iy_iz_i$ by performing a counterclockwise rotation about the x_i-axis by an angle α. The relevant coordinate transfer matrix is expressed as follows:

$$\left[C_{ij}{}^{(\alpha)}\right] = \begin{bmatrix} 1 & 0 & 0 \\ 0 & cos(\alpha) & sin(\alpha) \\ 0 & -sin(\alpha) & cos(\alpha) \end{bmatrix}$$

 doi:10.20944/preprints202407.1845.v1

Similarly, coordinate system $x_j y_j z_j$ is obtained from coordinate system $x_i y_i z_i$ by performing a counterclockwise rotation about the y_i-axis by an angle β (Figure 7). The relevant coordinate transfer matrix is expressed as follows:

$$[C_{ij}{}^{(\beta)}] = \begin{bmatrix} cos(\beta) & 0 & -sin(\beta) \\ 0 & 1 & 0 \\ sin(\beta) & 0 & cos(\beta) \end{bmatrix}$$

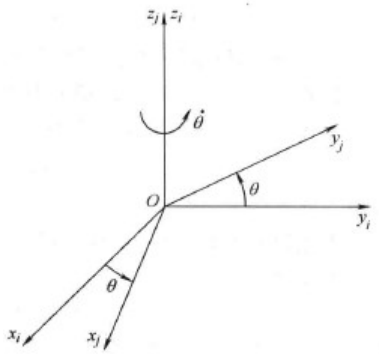

Figure 5. Rotation about the z_i-axis.

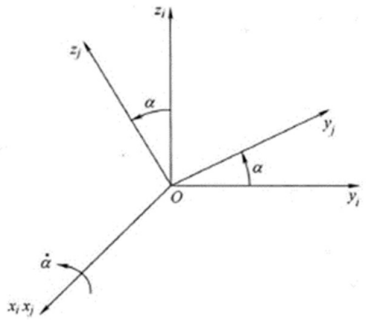

Figure 6. Rotation about the x_i-axis.

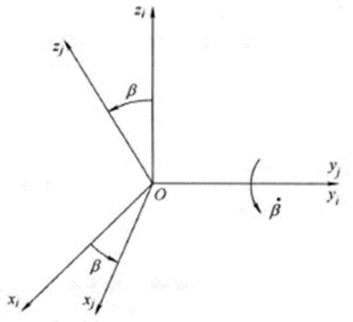

Figure 7. Rotation about the y_i-axis.

2.1.2. Multiple Rotations

As displayed in Figure 8, the orientation of the $x_j y_j z_j$ coordinate system relative to the $x_i y_i z_i$ coordinate system can be regarded as a transformation involving two steps. First, the $x_i y_i z_i$ coordinate system is rotated around the z_i-axis by θ, resulting in the $x_m y_m z_m$ coordinate system. The matrix relationship for this transformation is given as follows:

 doi:10.20944/preprints202407.1845.v1

$$\vec{r}_{x_m y_m z_m} = [C_{im}{}^{(\theta)}]\vec{r}_{x_i y_i z_i} = \begin{bmatrix} cos(\theta) & sin(\theta) & 0 \\ -sin(\theta) & cos(\theta) & 0 \\ 0 & 0 & 1 \end{bmatrix} \vec{r}_{x_i y_i z_i}, \quad (2)$$

where $\vec{r}_{x_i y_i z_i}$ is a vector in the $x_i y_i z_i$ coordinate system. This vector can be expressed in the $x_m y_m z_m$ coordinate system as $\vec{r}_{x_m y_m z_m}$ by using Equation (2).
Second, the $x_m y_m z_m$ coordinate system is rotated around the x_m-axis by an angle α to become the $x_j y_j z_j$coordinate system; the corresponding coordinate transformation matrix relationship can be expressed as follows:

$$\vec{r}_{x_j y_j z_j} = [C_{mj}{}^{(\alpha)}]\vec{r}_{x_m y_m z_m} = \begin{bmatrix} 1 & 0 & 0 \\ 0 & cos(\alpha) & sin(\alpha) \\ 0 & -sin(\alpha) & cos(\alpha) \end{bmatrix} \vec{r}_{x_m y_m z_m}, \quad (3)$$

where $\vec{r}_{x_m y_m z_m}$ is a vector in the $x_m y_m z_m$ coordinate system. This vector can be expressed in the $x_i y_i z_i$system as follows:

$$\vec{r}_{x_j y_j z_j} = [C_{mj}{}^{(\alpha)}]\vec{r}_{x_m y_m z_m} = [C_{mj}{}^{(\alpha)}][C_{im}{}^{(\theta)}]\vec{r}_{x_i y_i z_i}, \quad (4)$$

Equation (4) can be used to achieve continuous transformations between coordinate systems.

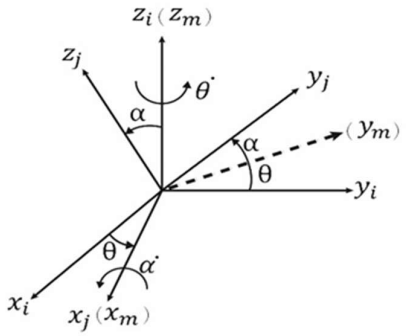

Figure 8. Coordinate transformation through rotation around two axes.

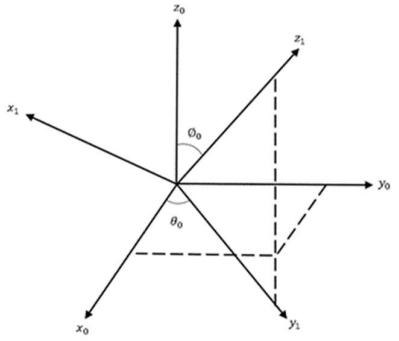

Figure 9. Relationship between the $x_0 y_0 z_0$ and $x_m y_m z_m$ coordinate systems.

If an axis of a reference frame is specified, its coordinate system can be conveniently selected, as shown in Figure 9. If z_1 is the specified axis of the system $x_0 y_0 z_0$, the polar and azimuthal angles are ϕ_0 and θ_0, respectively. First, the coordinate system $x_0 y_0 z_0$ is rotated around the z_0 -axis clockwise by an angle $\frac{\pi}{2} - \theta_0$, resulting in the $x_m y_m z_m$ coordinate system. Next, the $x_m y_m z_m$ coordinate system is rotated around the x_m-axis clockwise by an angle ϕ_0, transforming it into the $x_1 y_1 z_1$ coordinate system. Here, $\vec{r}_{x_0 y_0 z_0}$ is a vector in the $x_0 y_0 z_0$ coordinate system. This vector can be expressed in the $x_1 y_1 z_1$ coordinate system as follows:

 doi:10.20944/preprints202407.1845.v1

$$\vec{r}_{x_1y_1z_1} = \left[C_{m1}{}^{(-\phi_0)}\right]\left[C_{0m}{}^{\left(-\left(\frac{\pi}{2}-\theta_0\right)\right)}\right]\vec{r}_{x_0y_0z_0}, \tag{5}$$

2.1.3. Motion of the Driver-Side Linkage of the CDLS

The Z-axis of the XYZ coordinate system is aligned with the crankshaft axis, and the crank itself is positioned in the XY plane of this coordinate system. Assume that the unit vector of the main output shaft's axis Z_1 is $(cos(\theta_0)sin(\phi_0), sin(\theta_0)sin(\phi_0), cos(\phi_0))$. A reference coordinate system $X_1Y_1Z_1$ is defined for the main output shaft. Here, $\vec{r}_{XYZ}$ is a vector in the XYZ coordinate system. This vector can be expressed in the $X_1Y_1Z_1$ coordinate system as follows by using Equation (5):

$$\vec{r}_{X_1Y_1Z_1} = \begin{bmatrix} sin\theta_0 & -cos\theta_0 & 0 \\ cos\theta_0 cos\phi_0 & sin\theta_0 cos\phi_0 & -sin\phi_0 \\ sin\phi_0 cos\theta_0 & sin\phi_0 sin\theta_0 & cos\phi_0 \end{bmatrix}\vec{r}_{XYZ}, \tag{6}$$

$$\text{Let } \mathrm{R} = \begin{bmatrix} sin\theta_0 & -cos\theta_0 & 0 \\ cos\theta_0 cos\phi_0 & sin\theta_0 cos\phi_0 & -sin\phi_0 \\ sin\phi_0 cos\theta_0 & sin\phi_0 sin\theta_0 & cos\phi_0 \end{bmatrix}, \tag{7}$$

Assume that vectors $\overrightarrow{AB}$ and $\overrightarrow{AD}$ are defined as follows in the XYZ coordinate system:

$$\overrightarrow{AB} = \begin{bmatrix} r_2\cos(\theta_2) \\ r_2\sin(\theta_2) \\ 0 \end{bmatrix}, \overrightarrow{AD} = \begin{bmatrix} r_1\sin(\phi_1)\cos(\theta_1) \\ r_1\sin(\phi_1)\sin(\theta_2) \\ r_1\cos(\phi_1) \end{bmatrix}$$

Vector $\overrightarrow{AB} - \overrightarrow{AD}$ can then be expressed in the $X_1Y_1Z_1$ coordinate system as follows:

$$\begin{bmatrix} r_{2x} \\ r_{2y} \\ r_{2z} \end{bmatrix} = R\begin{bmatrix} r_2\cos\theta_2 \\ r_2\sin\theta_2 \\ 0 \end{bmatrix} - R\begin{bmatrix} r_1\sin\phi_1\cos\theta_1 \\ r_1\sin\phi_1\sin\theta_1 \\ r_1\cos\phi_1 \end{bmatrix}, \tag{8}$$

Similarly, assume that vectors $\overrightarrow{DC}$ and $\overrightarrow{BC}$ are defined as follows in the $X_1Y_1Z_1$ coordinate system:

$$\overrightarrow{DC} = \begin{bmatrix} r_4\cos(\theta_4) \\ r_4\sin(\theta_4) \\ 0 \end{bmatrix}, \overrightarrow{BC} = \begin{bmatrix} r_3sin(\phi_3)cos(\theta_3) \\ r_3\,sin(\phi_3)sin(\theta_3) \\ r_3\,cos(\phi_3) \end{bmatrix}$$

The following equality can be derived by considering Figure 3 and using the vector loop method:

$$\overrightarrow{AB} + \overrightarrow{BC} + \overrightarrow{CD} + \overrightarrow{DA} = \vec{0}\,, \tag{9}$$

Expressing this vector equality in terms of the $X_1Y_1Z_1$ coordinate system results in the following relations:

$$r_{2x} + r_3sin\phi_3cos\theta_3 - r_4cos\theta_4 = 0\,, \tag{10}$$

$$r_{2y} + r_3sin\phi_3sin\theta_3 - r_4sin\theta_4 = 0\,, \tag{11}$$

$$r_{2z} + r_3cos\phi_3 = 0\,, \tag{12}$$

The solution of Equation (12) is given as follows:

$$\phi_3 = cos^{-1}(r_{2z})\,, \tag{13}$$

Squaring Equations (10) and (11) and adding them results in the following relation without θ_3:

$$A\cos\theta_4 + B\sin\theta_4 + C = 0\,, \tag{14}$$

where $\mathrm{A} = 2r_4r_{2x}$, $\mathrm{B} = 2r_4r_{2y}$, and $\mathrm{C} = r_3{}^2sin\ \phi_3{}^2 - r_{2x}{}^2 - r_4{}^2 - r_{2y}{}^2$.

Let

 doi:10.20944/preprints202407.1845.v1

$$tan\frac{\theta_4}{2} = \beta$$

The half-angle formula for tangent can be used to express Equation (14) in the following form:

$$(C - A)\beta^2 + 2B\beta + (C + A) = 0\,, \tag{15}$$

The following expression is obtained by solving Equation (15) for β:

$$\beta = \frac{-B \pm \sqrt{B^2 - (C^2 - A^2)}}{(C - A)}$$

Thus, the following equation is obtained:

$$\theta_4 = 2 \cdot arctan\left(\frac{-B \pm \sqrt{B^2 - (C^2 - A^2)}}{(C - A)}\right), \tag{16}$$

In Equation (16), θ_4 has two solutions representing the motion of the linkage above or below the x_1-axis. The following solution is obtained for θ_4 when the positive square root is considered:

$$\theta_4 = 2 \cdot arctan\left(\frac{-B + \sqrt{B^2 - (C^2 - A^2)}}{(C - A)}\right), \tag{17}$$

The following expression is obtained by substituting Equation (17) into Equations (10) and (11):

$$\theta_3 = arctan\left(\frac{-r_{2y} + r_4 sin\theta_4}{-r_{2x} + r_4 cos\theta_4}\right), \tag{18}$$

The angular velocity ω_2 (the derivative of θ_2 with respect to time) of Link AB is fixed at 1 rad/s. The time derivatives of ϕ_3 (ϕ_3'), θ_3 (ω_3), and θ_4 (ω_4), which is the angular velocity of Link DC) for Link DC are obtained by differentiating Equations (10)–(12) with respect to time (t).

$$\phi_3{}' = \frac{r'_{2z}}{r_3 \sin(\phi_3)}, \tag{19}$$

$$w_3 = \frac{(r'_{2x}\cos(\theta_4) + r'_{2y}\sin(\theta_4)}{r_3 \sin(\phi_3)\sin(\theta_4 - \theta_3)} + \frac{r_3 cos\,(\phi_3) cos\,(\theta_3 - \theta_4)\phi_3{}'}{r_3 sin\,(\phi_3) sin\,(\theta_4 - \theta_3)}, \tag{20}$$

$$w_4 = \frac{-r'_{2x}\,cos(\theta_3) - r'_{2y}\,sin(\theta_3) - r_3\,cos(\phi_3)\phi'_3}{r_4 sin\,(\theta_4 - \theta_3)}, \tag{21}$$

The angular velocity of Link AB is fixed at 1 rad/s; therefore, the angular acceleration α_2 of this link is 0. Equations (10)–(12) are differentiated twice with respect to time (t) to obtain $\phi_3{}''$ from $\phi_3{}'$ α_3 from ω_3, and α_4 from ω_4 for Link DC; ω_4 is the angular acceleration of Link DC.

$$\phi''_3 = \frac{r_{2z}{}'' - r_3 \cos\phi_3 {\phi_3}^2}{r_3 \sin(\phi_3)}, \tag{22}$$

$$\alpha_3 = \frac{r''_{2x}\cos(\theta_4) + r''_{2y}\sin(\theta_4)}{r_3 \sin(\phi_3)\sin(\theta_3 - \theta_4)} - \frac{r_3 \sin(\phi_3){\phi_3}'^2 \cos(\theta_4 - \theta_3)}{r_3 \sin(\phi_3)\sin(\theta_3 - \theta_4)} + \frac{r_3 \cos(\phi_3)\phi''_3 \cos(\theta_4 - \theta_3)}{r_3 \sin(\phi_3)\sin(\theta_3 - \theta_4)} - \frac{r_3 \sin(\phi_3)\cos(\theta_4 - \theta_3){w_3}^2}{r_3 \sin(\phi_3)\sin(\theta_3 - \theta_4)} - \frac{2r_3 \cos(\phi_3)\phi'_3 w_3 \sin(\theta_3 - \theta_4)}{r_3 \sin(\phi_3)\sin(\theta_3 - \theta_4)} + \frac{r_4 {w_4}^2}{r_3 \sin(\phi_3)\sin(\theta_3 - \theta_4)}, \tag{23}$$

and

$$\alpha_4 = \frac{r''_{2x}\cos(\theta_3) + r''_{2y}\sin(\theta_3)}{r_4 \sin(\theta_3 - \theta_4)} + \frac{r_3 \cos(\phi_3)\phi''_3}{r_4 \sin(\theta_3 - \theta_4)} - \frac{(r_3 \sin(\phi_3){\phi_3}'^2 + r_3 \sin(\phi_3){w_3}^2)}{r_4 \sin(\theta_3 - \theta_4)} + \frac{r_4 {w_4}^2 \cos(\theta_4 - \theta_3)}{r_4 sin\,(\theta_3 - \theta_4)}, \tag{24}$$

The transmission angle μ_4 for the driver side of the CDLS can be expressed as follows by using the dot product of vectors CD and CB:

$$\mu_4 = \arccos\left(\frac{\overrightarrow{CD}\cdot\overrightarrow{CB}}{r_3 r_4}\right), \tag{25}$$

2.1.4. Motion of the Passenger-Side Linkage of the CDLS

Assume that the unit vector of the main output shaft's axis Z_2 is $(cos(\theta_{01})sin(\phi_{01}), sin(\theta_{01})sin(\phi_{01}), cos(\phi_{01}))$. An $X_2Y_2Z_2$ coordinate system is established on the

 doi:10.20944/preprints202407.1845.v1

auxiliary output shaft, where the Z_2- axis is aligned with the auxiliary output shaft's axis of rotation. The matrix relationship between the XYZ and $X_2Y_2Z_2$ coordinate systems is as follows:

$$\vec{r}_{X_2Y_2Z_2} = \begin{bmatrix} sin\theta_{01} & -cos\theta_{01} & 0 \\ cos\theta_{01}cos\phi_{01} & sin\theta_{01}cos\phi_{01} & -sin\phi_{01} \\ sin\phi_{01}cos\theta_{01} & sin\phi_{01}sin\theta_{01} & cos\phi_{01} \end{bmatrix} \vec{r}_{XYZ} \ , \tag{26}$$

$$\text{Let } R_1 = \begin{bmatrix} sin\theta_{01} & -cos\theta_{01} & 0 \\ cos\theta_{01}cos\phi_{01} & sin\theta_{01}cos\phi_{01} & -sin\phi_{01} \\ sin\phi_{01}cos\theta_{01} & sin\phi_{01}sin\theta_{01} & cos\phi_{01} \end{bmatrix} , \tag{27}$$

Assume that vectors $\overrightarrow{AB}$ and $\overrightarrow{AE}$ are defined as follows in the XYZ coordinate system:

$$\overrightarrow{AB} = \begin{bmatrix} r_2\cos(\theta_2) \\ r_2\sin(\theta_2) \\ 0 \end{bmatrix}, \overrightarrow{AE} = \begin{bmatrix} r_{11}\sin(\phi_{11})\cos(\theta_{11}) \\ r_{11}\sin(\phi_{11})\sin(\theta_{11}) \\ r_{11}\cos(\phi_{11}) \end{bmatrix}$$

The vector $\overrightarrow{AB} - \overrightarrow{AE}$ can be expressed in $X_2Y_2Z_2$ as

$$\begin{bmatrix} r_{21x} \\ r_{21y} \\ r_{21z} \end{bmatrix} = R_1 \begin{bmatrix} r_2\cos\theta_2 \\ r_2\sin\theta_2 \\ 0 \end{bmatrix} - R_1 \begin{bmatrix} r_{11}\sin\phi_{11}\cos\theta_{11} \\ r_{11}\sin\phi_{11}\sin\theta_{11} \\ r_{11}\cos\phi_{11} \end{bmatrix} , \tag{28}$$

Similarly, assume that vectors $\overrightarrow{EF}$ and $\overrightarrow{BF}$ are defined as follows in the $X_2Y_2Z_2$ coordinate system:

$$\overrightarrow{EF} = \begin{bmatrix} r_6\cos(\theta_6) \\ r_6\sin(\theta_6) \\ 0 \end{bmatrix}, \overrightarrow{BF} = \begin{bmatrix} r_5\sin(\phi_5)\cos(\theta_5) \\ r_5\sin(\phi_5)\sin(\theta_5) \\ r_5\cos(\phi_5) \end{bmatrix}$$

Similar mathematical formulas are valid for the motion of the passenger-side linkage of the CDLS. In this case, θ_2 is the input variable of the input link AB, and θ_6 is the unknown output of the output link EF. The following expressions are obtained by using the vector loop method and the half-angle formula for tangent:

$$\phi_5 = arccos(r_{21z}) \ , \tag{29}$$

$$\theta_6 = 2 \cdot arctan\left(\frac{-E \pm \sqrt{E^2-(F^2-D^2)}}{(F-D)}\right) , \tag{30}$$

$$\theta_5 = tan^{-1}\left(\frac{-r_{21y} + r_6 sin\theta_6}{-r_{21x} + r_6 cos\theta_6}\right) , \tag{31}$$

with $D = 2r_6r_{21x}, E = 2r_6r_{21y}$, and $F = {r_5}^2 sin\ {\phi_5}^2 - {r_{21}}^2 - {r_6}^2 - {r_{21y}}^2$.

The solution adopted for θ_6 is expressed as follows:

$$\theta_6 = 2 \cdot arctan\left(\frac{-E + \sqrt{E^2-(F^2-D^2)}}{(F-D)}\right) , \tag{32}$$

The time derivatives of ϕ_5 $({\phi_5}')$, θ_5 (ω_5), and θ_6 (ω_6), which is the angular velocity of Link EF) for Link EF are obtained as follows by using the method introduced in Section 2.1.3:

$${\phi_5}' = \frac{r'_{21z}}{r_5\sin(\phi_5)} , \tag{33}$$

$$\omega_5 = \frac{r'_{21x}cos(\theta_6) + r'_{21y}sin(\theta_6)}{(r_5 sin(\phi_5) sin(\theta_5 - \theta_6))} + \frac{r_5 cos(\phi_5) cos(\theta_5 - \theta_6){\phi_5}'}{(r_5 sin(\phi_5) sin(\theta_5 - \theta_6))} , \tag{34}$$

and

$$\omega_6 = \frac{-r'_{21x}cos(\theta_5) - r'_{21y}sin(\theta_5) - r_5 cos(\phi_5){\phi'}_5}{(r_6 sin(\theta_6 - \theta_5))} , \tag{35}$$

Similarly, the time derivatives of ${\phi_5}'$ $({\phi_5}'')$, ω_5 (α_5), and ω_6 (α_6), which is the angular acceleration of Link EF) for Link EF are expressed as follows:

 doi:10.20944/preprints202407.1845.v1

$$\phi_5'' = \frac{r_{21z}'' - r_5 \cos\phi_5 {\phi_5}^2}{r_5 \sin(\phi_5)}, \tag{36}$$

$$\alpha_5 = \frac{-r_{21x}'' cos(\theta_6) - r_{21y}'' sin(\theta_6)}{(r_5 sin(\phi_5) sin(\theta_5 - \theta_6))} + \frac{r_5 sin(\phi_5) {\phi_5}'^2 cos(\theta_5 - \theta_6)}{(r_5 sin(\phi_5) sin(\theta_5 - \theta_6))} - \frac{2 r_5 cos(\phi_5) \phi_5' w_5 sin(\theta_6 - \theta_5)}{(r_5 sin(\phi_5) sin(\theta_5 - \theta_6))} - \frac{r_5 cos(\phi_5) \phi_5'' cos(\theta_5 - \theta_6)}{(r_5 sin(\phi_5) sin(\theta_5 - \theta_6))} + \frac{r_5 sin(\phi_5) cos(\theta_5 - \theta_6) {w_5}^2}{(r_5 sin(\phi_5) sin(\theta_5 - \theta_6))} - \frac{r_6 {w_6}^2}{(r_5 sin(\phi_5) sin(\theta_5 - \theta_6))}, \tag{37}$$

$$\alpha_6 = \frac{r_{21x}'' cos(\theta_5) + r_{21y}'' sin(\theta_5)}{r_6 sin(\theta_5 - \theta_6)} - \frac{r_5 sin(\phi_5) {\phi_5}'^2}{r_6 sin(\theta_5 - \theta_6)} + \frac{r_5 cos(\phi_5) \phi_5'' - r_5 sin(\phi_5) {w_5}^2}{r_6 sin(\theta_5 - \theta_6)} + \frac{r_6 {w_6}^2 cos(\theta_5 - \theta_6)}{r_6 sin(\theta_5 - \theta_6)}, \tag{38}$$

The transmission angle μ_6 on the passenger side of the CDLS can then be expressed as follows:

$$\mu_6 = cos^{-1}\left(\frac{\overline{FE} \cdot \overline{FB}}{r_5 \times r_6}\right), \tag{39}$$

2.2. Dynamic Analysis of the Linkage System

In Figure 10, M_d represents the driving torque in the Z direction at point A. The terms M_{r4} and M_{r6} represent external torques at point D in the Z_1 direction and at point E in the Z_2 direction respectively; both have known magnitudes. The driving torque required for Link AB to maintain a constant angular velocity is calculated. The joint forces, bearing forces, and driving torque in the CDLS are derived using Newton–Euler equations of motion. To simplify the dynamic analysis model, the following three assumptions are made:

1. Friction at the joints can be neglected.
2. All links are rigid bodies.
3. The effects of gravity are negligible.
4. All links in the mechanism are homogeneous.

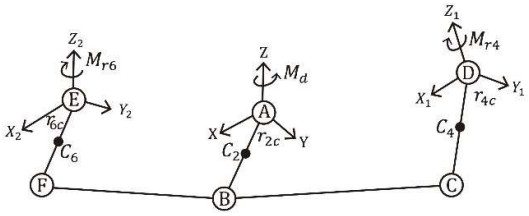

Figure 10. Simplified three-dimensional model of a CDLS.

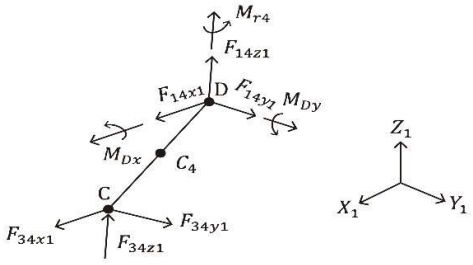

Figure 11. Free-body diagram of Link CD in the $X_1Y_1Z_1$ coordinate system.

In Figure 11, F_{14x1} F_{14y1}, and F_{14z1} represent the reaction forces in the X_1, Y_1, and Z_1 directions, respectively, at bearing D. The terms F_{34x1}, F_{34y1}, and F_{34z1} represent the components of the joint force exerted by Link BC on Link AB in the X_1, Y_1, and Z_1 directions. The masses of Links AB, BC, and CD are denoted by m_2, m_3, and m_4, respectively, and a_{4cx}, a_{4cy}, and a_{4cz} are the acceleration components of the center of mass C_4 of Link CD in each direction. The term I_4 represents the mass moment of inertia of Link CD relative to its center of mass, and M_{Dx} andM_{Dy} are

 doi:10.20944/preprints202407.1845.v1

the reaction moments in the X_1 and Y_1 directions, respectively, at bearing D. The position vector of the center of mass C_4 of Link CD is denoted by $\overrightarrow{DC_4}$ and expressed as follows:

$$\overrightarrow{DC_4} = (r_{4c}\,cos\theta_4\,, r_{4c}\,sin\,\theta_4\,, 0)\,, \tag{40}$$

where $\overrightarrow{a_4}$ is the acceleration of the center of mass C_4 of Link CD in the $X_1Y_1Z_1$ coordinate system.

$$\overrightarrow{a_{4c}} = \left(a_{4cx}, a_{4cy}, a_{4cz}\right), \tag{41}$$

Differentiating each component of vector $\overrightarrow{DC_4}$ with respect to t twice yields the following expressions:

$$a_{4cx} = -r_{4c}\,{\omega_4}^2 cos\theta_4 - r_{4c}\alpha_4\,sin\,\theta_4$$
$$a_{4cy} = -r_{4c}\,{\omega_4}^2 sin\theta_4 + r_{4c}\alpha_4\,\cos\theta_4$$
$$a_{4cz} = 0$$

Suppose that the force vector $\overrightarrow{F_{34}}$ is scaled by a factor of K in the direction of the unit vector of BC; that is,

$$\left(F_{34x1}, F_{34y1}, F_{34z1}\right) = K_1(sin\phi_3 cos\theta_3, sin\phi_3\,\sin\theta_3\,, cos\phi_3)$$

The force balance equations and torque equations are as follows :

$$F_{14x1} + F_{34x1} = m_4 a_{4cx}\,, \tag{42}$$

$$F_{14y1} + F_{34y1} = m_4 a_{4cy}\,, \tag{43}$$

$$F_{14z1} + F_{34z1} = m_4 a_{4cz}\,, \tag{44}$$

$$-F_{14z1} r_{4c}\,sin(\theta_4) + F_{34z1}(r_4 - r_{4c})\,sin(\theta_4) + M_{Dx} = 0\,, \tag{45}$$

$$F_{14z1} r_{4c}\,cos(\theta_4) - F_{34z1}(r_4 - r_{4c})\,cos(\theta_4) + M_{Dy} = 0\,, \tag{46}$$

$$F_{14x1} r_{4c}\,sin(\theta_4) - F_{14y1} r_{4c}\,cos(\theta_4) - F_{34x1}(r_4 - r_{4c})\,sin(\theta_4) + F_{34y1}(r_4 - r_{4c})\,cos(\theta_4) = I_4\alpha_4 - \mathrm{M}_{r4}\,, \tag{47}$$

Using the Equation (41), (42), (43), (44), (45) and (46) we may obtain $K_1, F_{14x1}, F_{14y}, F_{14z}, F_{34x1}, F_{34y1}, F_{34z1}, M_{Dx}$, and M_{Dy} as follow:

$$\begin{bmatrix} K_1 \\ F_{14x1} \\ F_{14y1} \\ F_{14z1} \\ F_{34x1} \\ F_{34y1} \\ F_{34z1} \\ M_{Dx} \\ M_{Dy} \end{bmatrix} = \begin{bmatrix} G_1 & 0 & 0 & 0 & 1 & 0 & 0 & 0 & 0 \\ G_2 & 0 & 0 & 0 & 0 & 1 & 0 & 0 & 0 \\ G_3 & 0 & 0 & 0 & 0 & 0 & 1 & 0 & 0 \\ 0 & 1 & 0 & 0 & 1 & 0 & 0 & 0 & 0 \\ 0 & 0 & 1 & 0 & 0 & 1 & 0 & 0 & 0 \\ 0 & 0 & 0 & 1 & 0 & 0 & 1 & 0 & 0 \\ 0 & 0 & 0 & G_4 & 0 & 0 & G_5 & 1 & 0 \\ 0 & 0 & 0 & G_6 & 0 & 0 & G_7 & 0 & 1 \\ 0 & G_8 & G_9 & 0 & G_{10} & G_{11} & 0 & 0 & 0 \end{bmatrix}^{-1} \begin{bmatrix} 0 \\ 0 \\ 0 \\ m_4 a_{4cx} \\ m_4 a_{4cy} \\ m_4 a_{4cz} \\ 0 \\ 0 \\ I_4\alpha_4 - M_{r_4} \end{bmatrix}, \tag{48}$$

in which $G_1 = -sin\phi_3 cos\theta_3, G_2 = -sin\phi_3 sin\theta_3, G_3 = -cos\phi_3, G_4 = -r_{4c} sin\theta_4$, $G_5 = (r_4 - r_{4c})sin\theta_4, G_6 = r_{4c} cos\theta_4, G_7 = -(r_4 - r_{4c})cos\theta_4$ and $G_8 = r_{4c} sin\theta_4$.

 doi:10.20944/preprints202407.1845.v1

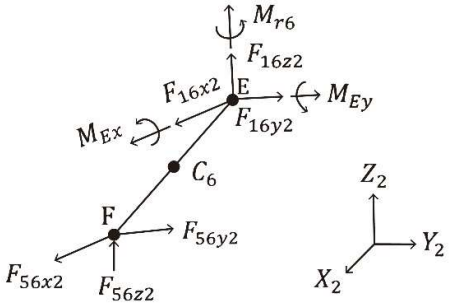

Figure 12. Free-body diagram of Link EF in the $X_2Y_2Z_2$ coordinate system.

In Figure 12, F_{16x2}, F_{16y}, and F_{16z2} represent the reaction forces in the X_2, Y_2, and Z_2 directions, respectively, at bearing E. Moreover, F_{56x2}, F_{56y2}, and F_{56z2} are the components of the joint force exerted by Link BF on Link EF in the X_2, Y_2, and Z_2 directions, respectively. The terms a_{6cx}, a_{6cy}, and a_{6cz} represent the acceleration components of the center of mass C_6 of Link EF in the X_2, Y_2, and Z_2 directions, respectively. The term I_6 denotes the mass moment of inertia of Link EF relative to its center of mass; M_{Ex} and M_{Ey} are the reaction moments in the X_2 and Y_2 directions, respectively, at bearing E; and m_5 and m_6 represent the masses of Links BF and EF, respectively.

The following matrix can be obtained in the $X_2Y_2Z_2$ coordinate system by using the same method as that used for Figure 11:

$$\begin{bmatrix} K_2 \\ F_{16x2} \\ F_{16y2} \\ F_{16z2} \\ F_{56x2} \\ F_{56y2} \\ F_{56z2} \\ M_{Ex} \\ M_{Ey} \end{bmatrix} = \begin{bmatrix} H_1 & 0 & 0 & 0 & 1 & 0 & 0 & 0 & 0 \\ H_2 & 0 & 0 & 0 & 0 & 1 & 0 & 0 & 0 \\ H_3 & 0 & 0 & 0 & 0 & 0 & 1 & 0 & 0 \\ 0 & 1 & 0 & 0 & 1 & 0 & 0 & 0 & 0 \\ 0 & 0 & 1 & 0 & 0 & 1 & 0 & 0 & 0 \\ 0 & 0 & 0 & 1 & 0 & 0 & 1 & 0 & 0 \\ 0 & 0 & 0 & H_4 & 0 & 0 & H_5 & 1 & 0 \\ 0 & 0 & 0 & H_6 & 0 & 0 & H_7 & 0 & 1 \\ 0 & H_8 & H_9 & 0 & H_{10} & H_{11} & 0 & 0 & 0 \end{bmatrix}^{-1} \begin{bmatrix} 0 \\ 0 \\ 0 \\ m_6 a_{6cx} \\ m_6 a_{6cy} \\ m_6 a_{6c} \\ 0 \\ 0 \\ I_6\alpha_6 - M_{r_6} \end{bmatrix}, \quad (49)$$

in which $H_1 = -sin\phi_5 cos\theta_5, H_2 = -sin\phi_5 sin\theta_5, H_3 = -cos\phi_5, H_4 = -r_{6c} sin\theta_6,$
$H_5 = (r_6 - r_{6c})sin\theta_6, H_6 = r_{6c} cos\theta_6, H_7 = -(r_6 - r_{6c})cos\theta_6,\ H_8 = r_{6c} sin\theta_6, H_9 = -r_{6c} cos\theta_6$

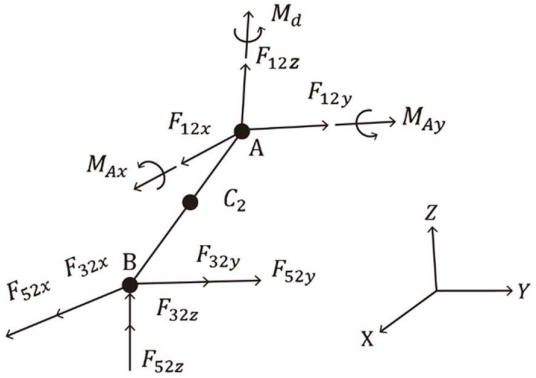

Figure 13. Free-body diagram of Link AB in the XYZ coordinate system.

$$\text{Let } \begin{bmatrix} F_{32x} \\ F_{32y} \\ F_{32z} \end{bmatrix} = R^{-1} \begin{bmatrix} F_{32x1} \\ F_{32y1} \\ F_{32z1} \end{bmatrix} \quad \text{and} \quad \begin{bmatrix} F_{52x} \\ F_{52y} \\ F_{52z} \end{bmatrix} = {R_1}^{-1} \begin{bmatrix} F_{52x2} \\ F_{52y2} \\ F_{52z2} \end{bmatrix}$$

 doi:10.20944/preprints202407.1845.v1

In Figure 13, F_{12x}, F_{12y}, and F_{12z} represent the reaction forces in the X, Y, and Z directions, respectively, at bearing A. The acceleration components of the center of mass C_2 of Link AB in the X, Y, and Z directions are a_{2cx}, a_{2cy}, and a_{2c}, respectively. The term I_2 represents the mass moment of inertia of Link AB relative to its center of mass. Moreover, M_{Ax} and M_{Ay} are the reaction moments in the X and Y directions, respectively, at bearing A. The following matrix is obtained in the XYZ coordinate system by using the same method as that used for Figure 11:

$$\begin{bmatrix} F_{12x} \\ F_{12y} \\ F_{12z} \\ M_{Ax} \\ M_{Ay} \\ M_d \end{bmatrix} = \begin{bmatrix} 0 & 0 & J_1 & 1 & 0 & 0 \\ 0 & 0 & J_2 & 0 & 1 & 0 \\ J_3 & J_4 & 0 & 0 & 0 & 1 \\ 1 & 0 & 0 & 0 & 0 & 0 \\ 0 & 1 & 0 & 0 & 0 & 0 \\ 0 & 0 & 1 & 0 & 0 & 0 \end{bmatrix}^{-1} \begin{bmatrix} -(F_{32z} + F_{52z})(r_2 - r_{2c})sin\theta_2 \\ (F_{32z} + F_{52z})(r_2 - r_{2c})cos\theta_2 \\ I_2\alpha_2 + (F_{32x} + F_{52x})(r_2 - r_{2c})sin\theta_2 - (F_{34y} + F_{52y})(r_2 - r_{2c})cos\theta_2 \\ m_2 a_{2cx} - (F_{32} + F_{52x}) \\ m_2 a_{2cy} - (F_{32} + F_{52y}) \\ m_2 a_{2cz} - (F_{32z} + F_{52z}) \end{bmatrix} \quad (50)$$

in which $J_1 = -r_{2c}\sin\theta_2$, $J_2 = r_{2c}\cos\theta_2$, $J_3 = r_{2c}\sin\theta_2$, and $J_4 = -r_{2c}\cos\theta_2$.

2.3. Optimization of the Angular Acceleration of the Output Links of the CDLS

DE is applied to maximize the angular acceleration of the output links of the designed CDLS for windshield wipers. The objective function f is as shown in equation (1).

A detailed explanation of the model is presented in Section 2.1. The input link AB of the designed CDLS is assumed to rotate at a constant angular velocity ω_2 = 1 rad/s, as illustrated in Figure 4. Relevant items are recorded or calculated at an interval of $\pi/180$ seconds. The widths of the wiping regions on the driver and passenger sides of the CDLS are $85\pi/180$ and $80\pi/180$ rad, respectively, with the permitted error margin being $1\pi/1800$ rad. The patterns of the wiping region are regulated in accordance with the guidelines provided in [14].

DE is employed to minimize *f* subject to 10 constraints. For the CDLS, the fixed constants are r_1 = 233.9 mm, r_{11}= 232.4 mm, ω_2 = 1 rad/sec, α_2= 0 rad/s², and r_2= 50 mm. Table 1 presents detailed information on the angle-related parameters used in the simulations. The constraints for the objective function f are listed as follows:

Table 1. Angle-related parameters used in simulations.

θ_1(rad)	ϕ_1(rad)	θ_{11}(rad)	ϕ_{11}(rad)	θ_0(rad)	ϕ_0(rad)	θ_{01}(rad)	ϕ_{01}(rad)
0.2279	1.6961	2.8886	1.6236	0	0	0.1368	0.1301

(1) $190 \le r_3 \le 400$ (mm)

(2) $50 \le r_4 \le 80$ (mm)

(3) $190 \le r_5 \le 400$ (mm)

(4) $50 \le r_6 \le 80$ (mm)

(5) $\left| \max_{0\le\theta_2\le2\pi} \theta_4 - \min_{0\le\theta_2\le2\pi} \theta_4 - \frac{85\pi}{180} \right| \le \frac{0.1\pi}{180}$ (rad)

(6) $\frac{40}{180} \le \mu_4 \le \frac{140\pi}{180}$ (rad)

(7) $|\omega_4| \le 0.3\pi$ (rad/s)

(8) $\left| \max_{0\le\theta_2\le2\pi} \theta_6 - \min_{0\le\theta_2\le2\pi} \theta_6 - \frac{80\pi}{180} \right| \le \frac{0.1\pi}{180}$ (rad)

(9) $\frac{40\pi}{180} \le \mu_6 \le \frac{140\pi}{180}$ (rad)

(10) $|\omega_6| \le 0.3\pi$ (rad/s)

The parameter values for DE in this study are as follows:

(1) Crossover ratio CR = 0.6.

(2) Scale factor F = 0.6.

(3) Population size M = 150.

(4) Maximum number of iterations G_{max} = 100.

 doi:10.20944/preprints202407.1845.v1

3. Results

Section 3.1 discusses the validation of our modeling approach. The results obtained from calculations using the mathematical formulas derived in Section 2.1 and those from the commercial software ADAMS were compared to validate the proposed model. Section 3.2 presents the optimized results obtained after using the DE method.

3.1. Comparison with ADAMS Results

We used MATLAB to calculate α_3, α_4, α_5, and α_6 in accordance with the formulas derived in Section 2.1. The calculated parameter values are listed in Table 1 and Table 2. The time interval and sampling time for the MATLAB computations were $[0, 2\pi]$ and $\pi/180$, respectively. The initial value of θ_2 was 0°.

Table 2. Length, angular velocity, and angular acceleration parameters used in simulations.

r_1(mm)	r_{11}(mm)	r_3(mm)	r_4(mm)	r_5(mm)	r_6 (mm)	α_2(rad/sec^2)	w_2 (rad/sec)
233.9	232.4	229.9	71.4	227.5	75.1	0	1

To validate the proposed model, the simulation parameters used in MATLAB were also input into the commercial software ADAMS. Figures 14–17 present a comparison between the results obtained from MATLAB and ADAMS for α_3, α_4, α_5, and α_6, respectively.

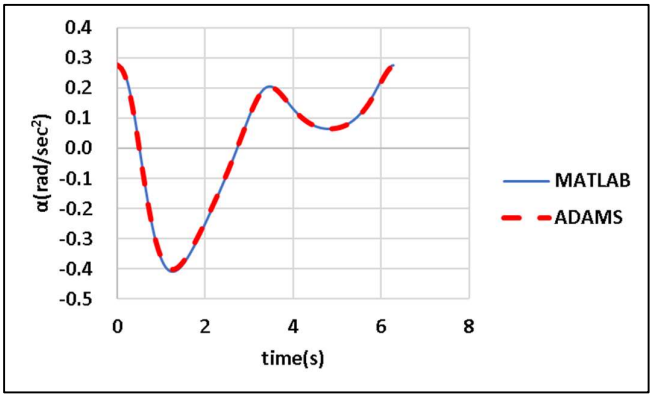

Figure 14. Comparison of the MATLAB and ADAMS results for α_3.

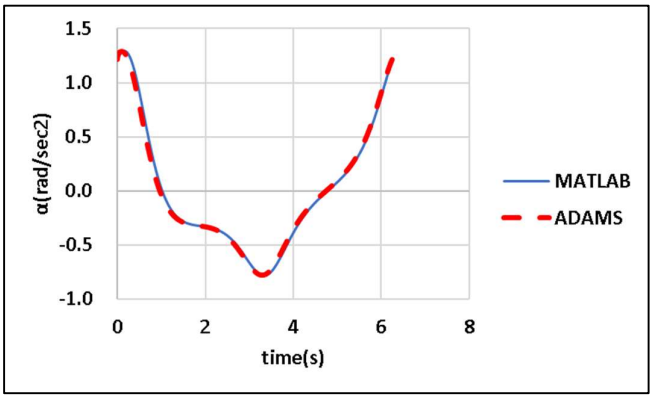

Figure 15. Comparison of the MATLAB and ADAMS results for α_4.

Preprints.org (www.preprints.org) | NOT PEER-REVIEWED | Posted: 24 July 2024 doi:10.20944/preprints202407.1845.v1

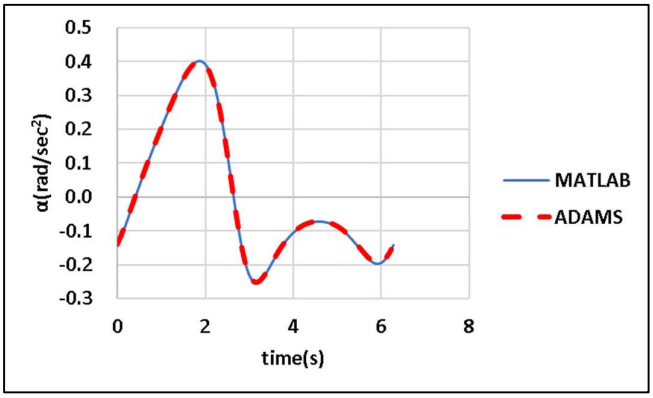

Figure 16. Comparison of the MATLAB and ADAMS results for α_5.

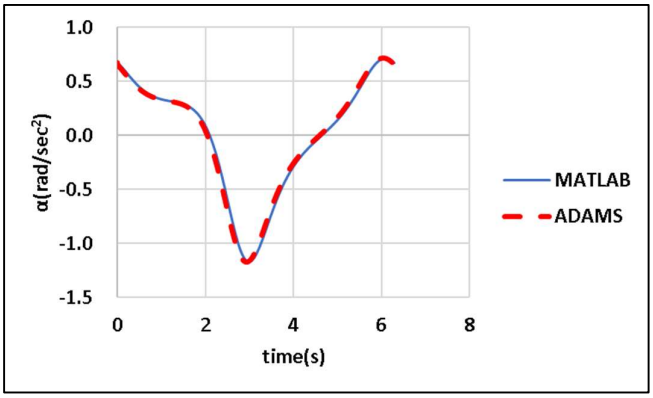

Figure 17. Comparison of the MATLAB and ADAMS results for α_6.

We calculated F_{12x} , F_{12y} , F_{12z} and M_d MATLAB by using the formulas derived in Section 2.2. The parameter values used in the calculations are listed in Tables 1, 2, and 3. To validate the proposed model, we input the same parameters into the commercial software ADAMS. Figures 18–21 depict the MATLAB and ADAMS results obtained for F_{12x} , F_{12y} , F_{12z} and M_d respectively.

Table 3. Parameter values used in simulations.

m_2(kg)	m_4(kg)	m_6(kg)	I_2(kg-mm^2)	I_4(kg-mm^2)	I_6(kg-mm^2)	M_{r4}(N-m)	M_{r6}(N-m)
0.204	0.271	0.283	13.194	17.650	18.415	15	15

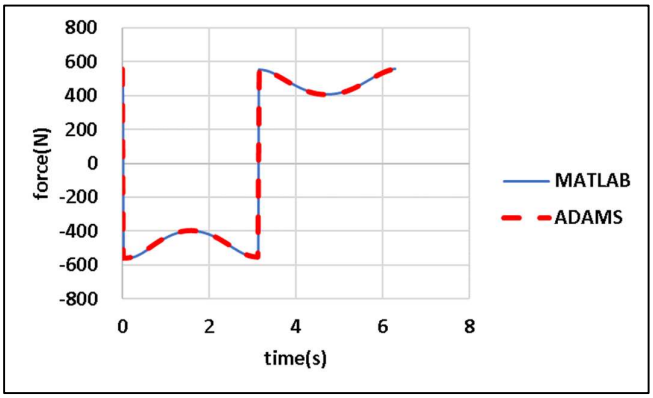

Figure 18. Comparison of the MATLAB and ADAMS results for F_{12x}.

Preprints.org (www.preprints.org) | NOT PEER-REVIEWED | Posted: 24 July 2024 doi:10.20944/preprints202407.1845.v1

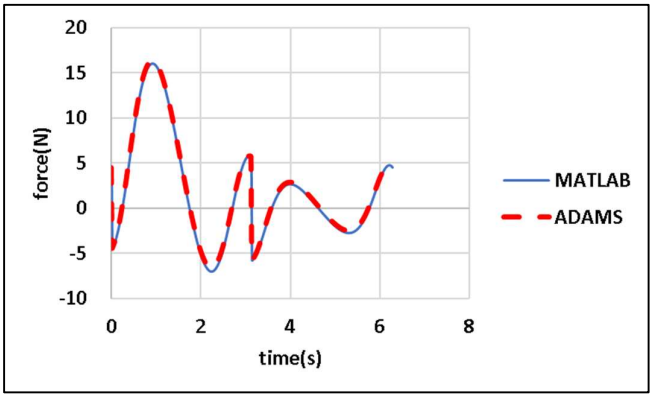

Figure 19. Comparison of of the MATLAB and ADAMS results for F_{12y}.

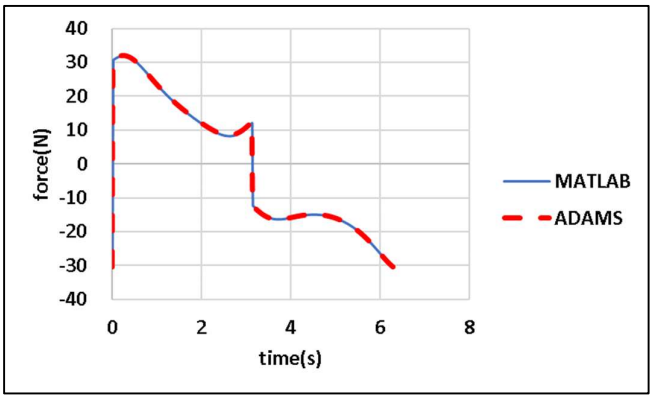

Figure 20. Comparison of the MATLAB and ADAMS results for F_{12z}.

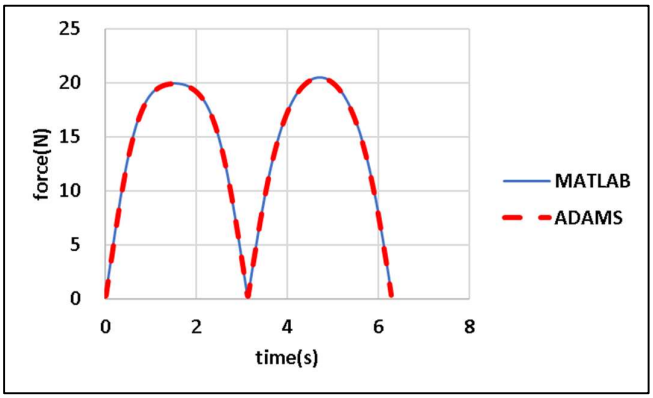

Figure 21. Comparison of the MATLAB and ADAMS results for M_d.

A comparison of the results calculated with MATLAB and those obtained from ADAMS suggest that our modeling method is accurate and reliable.

3.2. DE Results for Linkage Length Optimization

Table 4 presents the optimized linkage lengths obtained after DE for minimizing the absolute angular accelerations $|\alpha_4|$ and $|\alpha_6|$ of the CDLS.

Table 4. Linkage lengths before and after DE optimization.

	r_3(mm)	r_4(mm)	r_5 (mm)	r_6 (mm)
Linkage length before DE	229.9	71.4	227.5	75.1
Linkage length after DE	228.9	74.1	224.1	76.4

Preprints.org (www.preprints.org) | NOT PEER-REVIEWED | Posted: 24 July 2024 doi:10.20944/preprints202407.1845.v1

Figures 22 and 23 reveal that DE optimization decreased the maximal absolute values of α_4 and α_6 of the output links on the driver and passenger sides of the CDLS.

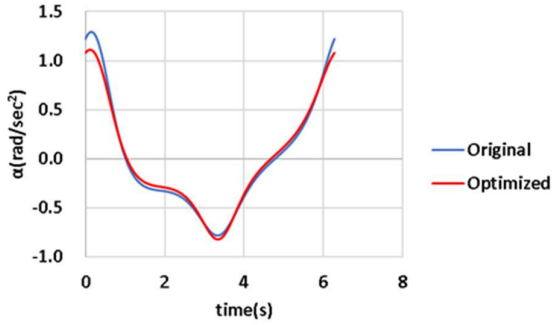

Figure 22. Optimized and unoptimized angular acceleration α_4 of the driver-side output link of the CDLS.

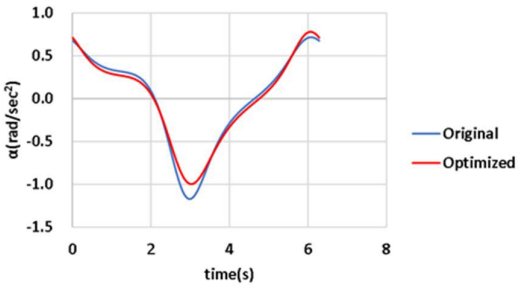

Figure 23. Optimized and unoptimized angular acceleration α_6 of the passenger-side output link of the CDLS.

Figures 24–26 reveal that the transmission angles were closer to $90°$ after optimization, which slightly reduced the maximum motor driving torque.

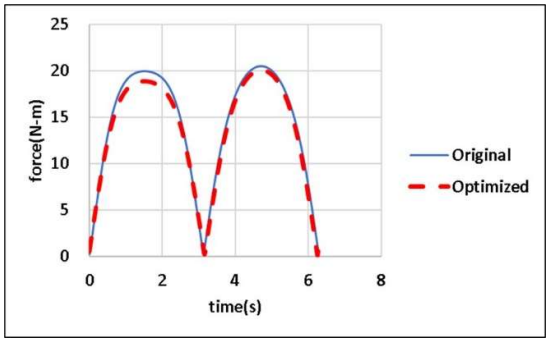

Figure 24. Motor driving torque M_d before and after DE optimization.

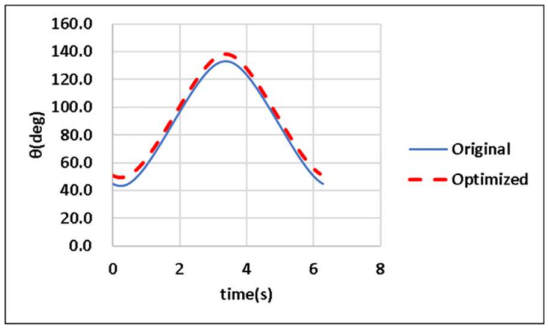

Figure 25. Ttransmission angle μ_4 for the driver-side output link of the CDLS before and after DE optimization.

 doi:10.20944/preprints202407.1845.v1

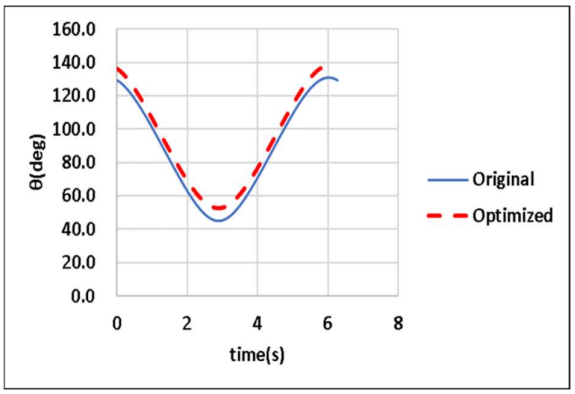

Figure 26. Transmission angle μ_6 for the passenger-side output link of the CDLS before and after DE optimization.

Tables 5 and 6 presents the values of various parameters before and after DE optimization. Optimization reduced the maximum angular accelerations of the driver- and passenger-side output links of the CDLS ($\max|\alpha_4|$ and $\max|\alpha_6|$ respectively) by 13.64% and 14.38%, respectively.

Table 5. Values of α_4 and ω_4 for the driver-side output link of the CDLS before and after DE optimization.

	$\max_{0\le\theta_2\le2\pi}\alpha_4$	$\min_{0\le\theta_2\le2\pi}\alpha_4$	$\max_{0\le\theta_2\le2\pi}\omega_4$	$\min_{0\le\theta_2\le2\pi}\omega_4$
Before DE	1.290	-0.783	0.787	-0.701
After DE	1.114	-0.825	0.728	-0.683
Change	-13.64%	5.36%	-7.50%	-2.57%

Table 6. Values of α_6 and ω_6 for the passenger-side output link of the CDLS before and after DE optimization.

	$\max_{0\le\theta_2\le2\pi}\alpha_6$	$\min_{0\le\theta_2\le2\pi}\alpha_6$	$\max_{0\le\theta_2\le2\pi}\omega_6$	$\min_{0\le\theta_2\le2\pi}\omega_6$
Before DE	0.716	-1.168	0.742	-0.667
After DE	0.782	-1.000	0.681	-0.651
Change	9.21%	-14.38%	-8.22%	-2.40%

4. Discussion

In this study, we successfully established the kinematics of a three-dimensional CDLS for windshield wipers. We designed a method for enhancing the stability of the system while maintaining its functionality. This improvement was achieved by minimizing the maximal absolute angular acceleration of the system's output links through DE optimization. The designed method was applied to a commercially available CDLS for vehicle wipers. We also developed a dynamic model of the center-driven linkage to determine the driving torque required from the motor to maintain constant crank rotation under a fixed frictional resistance torque.

In future research, we plan to use the Ansys/Fluent software program to perform numerical simulations of the wiper blade's interaction with the windshield to obtain lift and drag coefficients. Moreover, we intend to incorporate a wiper arm into the current CDLS model to simulate the forces during wiper operation on a glass surface with a given friction coefficient. This approach will provide a more accurate description of the wiper linkage system's dynamic behavior.

 doi:10.20944/preprints202407.1845.v1

Author Contributions: Methodology, T.-J.C.; Software ,Tien-Shun Chung .

Data Availability Statement: Not applicable.

Conflicts of Interest: The authors declare that they have no conflict of interest.

References

1. Freudenstein, F.; Kiss, I.S. Type Determination of Skew Four-bar Mechanisms. *ASME J. Eng. Ind.* 1969, 91, 220–223.
2. Sticher, F.C.O. Mobility Limit Analysis of RSSR Mechanisms by "Ellipse diagram". Journal of Mechanisms 1970, 5(3), 393–415.
3. Bottema, O. The Motion of the Skew Four-bar. Journal of Mechanisms 1971, 6(1), 69–79.
4. Hamid, S.; Soni, A.H. Design of an RSSR Crank-rocker Mechanism for Optimum Force Transmission. In Proceedings of the 2nd OSU Applied Mechanisms Conference, 1971, 17; pp. 171–176.
5. Freudenstein, F.; Primrose, E. On the Criteria for the Rotatability of the Cranks of Skew Four-bar Linkage. Trans. ASME, J. Eng. Ind. 1976, 98(4), 1285–1288.
6. Alizade, R.A.; Freudenstein, F.; Pamidie, P.R. Optimum Path Generation by Means of the Sew Four-bar linkage. Mechanism and Machine Theory 1976, 11(4), 295–302.
7. Balaji, R.L.V.; Lakshminarayana, K. Optimal Designs of the RSSR Crank-rocker Mechanism-1. General time ratio. Mechanism and Machine Theory 1984, 19(4–5), 431–441.
8. Zhang, W.; Zhang, D. Conditions of Crank Existence for a Particular Case of the RSSR Linkage. Mechanism and Machine Theory 1993, 28(6), 845–850.
9. Söylemez, E. Transmission Optimization of Right-angled Four-bar Mechanisms. Mechanism and Machine Theory 1993, 28(4), 539–552.
10. Saka, Z. The RSSR Mechanisms with Partially Constant Transmission Angle. Mechanism and Machine Theory 1996, 31(6), 763–769.
11. Chung, W.Y. Mobility Analysis of RSSR Linkage and Type Maps of Special Cases. Mechanism and Machine Theory 2004, 39(4), 379–393.
12. Mirja Rotzolla.; Margaret H. Reganb.; Manfred L. Hustyc.; M. John D. Hayesa. Kinematic Geometry of Spatial RSSR Mechanisms, Mechanism and Machine Theory 2023, 185,p105335.
13. Chen, T.-J.; Hong, Y.-J. Geometric Analysis of the Vibration of Rubber Wiper Blade. Taiwanese Journal of Mathematics 2021, 25, 491–516.
14. Chen, T.-J.; Hong, Y.-J.; Lin, C.-H.; Wang, J.-Y. Optimization on Linkage System for Vehicle Wipers by the Method of Differential Evolution. Applied Sciences 2023, 13(1), 1-19.
15. Storn, R.; Price, K.V. Differential Evolution—A Simple and Efficient Adaptive Scheme for Global Optimization over Continuous Spaces; Technical Report, TR-95-012; International Computer Science Institute (ICSI) of University of California: Berkeley, CA, USA, 1995.
16. Storn, R.; Price, K.V. Differential Evolution—A Simple and Efficient Heuristic for Global Optimization over Continuous Spaces. J. Glob. Optim. 1997, 11, 341–359.
17. Storn, R.; Price, K.V.; Lampinen, J.A. Differential Evolution: A Practical Approach to Global Optimization; Springer: Berlin/Heidelberg, Germany, 2005.
18. Fan, Y.-F.; Lampinen, J. A Trigonometric Mutation Operation to Differential Evolution. Journal of Global Optimization 2003, 27(1), 105–129.
19. Tizhoosh, H.R. Opposition-Based Learning: A New Scheme for Machine Intelligence. In Proceedings of the International Conference on Computational Intelligence for Modelling, Control and Automation, Vienna, Austria, 28–30 November 2005; pp. 695–701.
20. Tizhoosh, H.R. Reinforcement Learning Based on Actions and Opposite Actions. In Proceedings of the ICGST International Conference on Artificial Intelligence and Machine Learning (AIML-05), Cairo, Egypt, 19-21 December 2005.
21. Tizhoosh, H.R. Opposition-based Reinforcement Learning. Journal of Advanced Computational Intelligence and Intelligent Informatics 2006, 10(4), 578–585.
22. Das, S.; Abraham, A.; Chakraborty, U.K.; Konar, A. Differential Evolution using a Neighborhood Based Mutation Operator. IEEE Transactions on Evolutionary Computation 2009, 13(3), 526–553.
23. Qin, A.K.; Huang, V.L.; Suganthan, P.N. Differential Evolution Algorithm with Strategy Adaptation for Global Numerical Optimization. IEEE Transactions on Evolutionary Computation 2009, 13(2), 398–417.
24. Brest, J.; Sepesy Maučec, M. Self-Adaptive Differential Evolution Algorithm Using Population Size Reduction and Three Strategies. Soft Computing 2011, 15(11), 2157–2174.
25. Lou, Y.; Yuen, S.Y.; Chen, G. Non-Revisiting Stochastic Search Revisited: Results, Perspectives, and Future Directions. Swarm and Evolutionary Computation 2021, 61, 100828.
26. Faramarzi, A.; Heidarinejad, M.; Mirjalili, S.; Gandomi, A.H. Equilibrium Optimizer: A Novel Optimization Algorithm. Knowl.-Based Syst. 2020, 191, 105190

 doi:10.20944/preprints202407.1845.v1

27. Mallipeddi, R.; Suganthan, P.N.; Pan, Q.K.; Tasgetiren, M.F. Differential Evolution Algorithm with Ensemble of Parameters and Mutation Strategies. *Appl. Soft Comput.* 2010, *11*, 1679-1696.
28. Wang, H.; Wu, Z.J.; Rahnamayan, S.; Kang, L.S. A Scalability Test for Accelerated DE Using Generalized Opposition-based Learning. In Proceedings of the International Conference on Intelligent System Design and Applications, Location, Country, 2009; pp. 1090-1095.
29. Choi, T.J.; Togelius, J.; Cheong, Y.G. A Fast and Efficient Stochastic Opposition-Based Learning for Differential Evolution in Numerical Optimization. Swarm Evol. Comput. 2021, 60, 100768.
30. Heidari, A.A.; Abbaspour, R.A.; Mirjalili, S. Harris hawks Optimization: Algorithm and Applications. *Future Gener. Comput. Syst.* 2019, *97*, 849-872.
31. Balli, S.S.; Chand, S. Transmission Angle in Mechanisms. Mech. Mach. Theory 2002, 37, 175–195.